

Learning Temporal Distribution and Spatial Correlation for Universal Moving Object Segmentation

Guanfang Dong*
University of Alberta
guanfang@ualberta.ca

Chenqiu Zhao*
University of Alberta
zhao.chenqiu@ualberta.ca

Xichen Pan
University of Alberta
xichen3@ualberta.ca

Anup Basu
University of Alberta
basu@ualberta.ca

Abstract

Universal moving object segmentation aims to provide a general model for videos from all types of natural scenes, as previous approaches are usually effective for specific or similar scenes. In this paper, we propose a method called **Learning Temporal Distribution and Spatial Correlation (LTS)** that has the potential to be a general solution for universal moving object segmentation. In the proposed approach, the distribution from temporal pixels is first learned by our **Defect Iterative Distribution Learning (DIDL)** network for a scene-independent segmentation. Then, the **Stochastic Bayesian Refinement (SBR)** Network, which learns the spatial correlation, is proposed to improve the binary mask generated by the **DIDL** network. Benefiting from the scene independence of the temporal distribution and the accuracy improvement resulting from the spatial correlation, the proposed approach performs well for almost all videos from diverse and complex natural scenes with fixed parameters. Comprehensive experiments on standard datasets including **LASIESTA**, **CDNet2014**, **BMC**, **SBMI2015** and 128 real world videos demonstrate the superiority of proposed approach compared to state-of-the-art methods with or without the use of deep learning networks. To the best of our knowledge, this work has high potential to be a general solution for moving object segmentation in real world environments. The code and real-world videos will be made public after the paper is accepted.

1. Introduction

Moving object segmentation for stationary cameras is a fundamental problem in computer vision that has been studied for several decades. While recent work based on deep learning networks [29] have achieved impressive results on

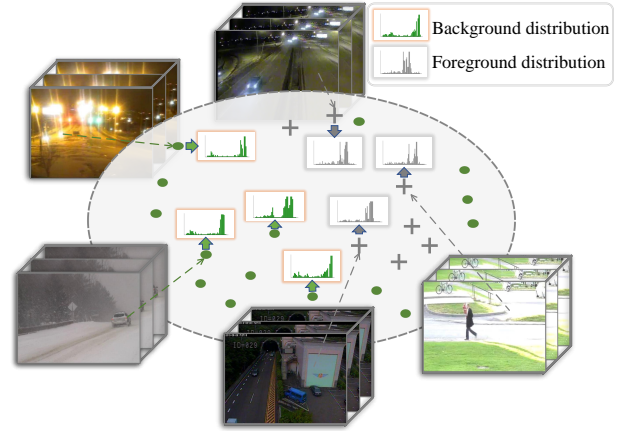


Figure 1: Illustration of the possibility of proposing a universal method for videos from diverse scenes. Although the scene information from different videos is completely different, the distributions of temporal pixels belonging to foreground or background are similar.

standard datasets, these models often require a tuning processes, such as data augmentation or network retraining, to perform well on new data. In practice, given the computational cost and uncertainty about the resulting performance, it is often difficult for users to obtain ground-truth frames for network retraining or follow complex instructions for data augmentation. Thus, proposing a universal method, which is directly applicable for moving object segmentation remains a challenging problem. In this work, we propose a novel method called **Learning Temporal distribution and Spatial correlation (LTS)**, which has a high potential to be a general solution for this challenge.

The proposed approach is different from previous scene-based networks. Our first focus is on learning distribution information, which is relatively less diverse due to the similarity of temporal pixel distributions across different videos,

*Equal contribution

as shown in Figure 1. Although the scene information in different videos may be completely different, the distribution information from temporal pixels is similar. This inspired us to propose a single network for learning distribution information from diverse videos, namely the Defect Iterative Distribution Learning (DIDL) network. Furthermore, temporal distributions can be sensitive to noise due to the independence in the spatial domain. To address this issue, we propose the Stochastic Bayesian Refinement (SBR) network to learn the spatial correlation for refining the generated binary mask. With temporal distribution learned by the DIDL network and the spatial correlation learned by the SBR network, the proposed LTS model has the potential for universal moving object segmentation.

The Defect Iterative Distribution Learning (DIDL) network and the Stochastic Bayesian Refinement (SBR) network are designed to address two key challenges. The first challenge is the very large number of temporal distributions, which leads to high computational cost during network training. To address this problem, we propose a defect iterative distribution learning strategy that uses parameters learned from a subset of the training set to approximate the parameters learned if the entire training set were used. In particular, these parameters are used to describe the temporal distributions. With the help of DIDL, the training of the proposed approach can be done within 48 hours based on over billion of training instances, using an Nvidia RTX A4000 GPU. The second challenge is the sensitivity of temporal distributions to noise. In order to improve the accuracy, spatial correlation is helpful, but training the network with spatial information often results in overfitting to specific scenes, thereby reducing the universality. To address this issue, we propose the Stochastic Bayesian Refinement network in which spatial pixels are stochastically sampled at multiple scales to prevent network overfitting. The main contributions of this paper are:

- We propose the Defect Iterative Distribution Learning (DIDL) network, which learns the distributions of temporal pixels for universal moving object segmentation. The DIDL network enables more efficient and effective learning for temporal pixel distributions.
- We propose the Stochastic Bayesian Refinement (SBR) network, which learns the correlation between spatial pixels to improve the segmentation results. The SBR network removes noise while maintaining universality, making it a valuable contribution to the field of universal moving object segmentation.
- We conduct comprehensive experiments on several standard datasets to demonstrate the superiority of our proposed approach compared to state-of-the-art methods, including both deep learning and non-deep learning methods. In addition, the proposed approach is

also tested on 128 videos of real life scenes, demonstrating the efficiency of the proposed approach in real applications.

2. Related Work

2.1. Non-Deep-Learning Methods

Approaches that do not use deep learning networks primarily focus on modeling the information in temporal pixels [3, 4, 5, 7, 8, 11, 12, 16, 19, 21, 22, 24, 27, 37, 38, 40, 41, 42, 55]. For instance, the Gaussian mixture model (GMM) proposed by Zivkovic et al. [55] models temporal pixels by several Gaussian functions, which was extended by several methods [5, 16]. Lee et al. [26] introduced an adaptive GMM of dynamic distributions, while Haines and Xiang [18] presented a GMM that uses a Dirichlet process. In addition to GMM, Chen et al. [8] learned models where adjacent pixels in different frames share models dynamically, while Berjon [3] proposed a non-parametric model using kernel density estimation and auxiliary tracking. Bianco et al. [4] proposed IUTIS-5, which selects the best-performing algorithm by genetic programming.

Unfortunately, due to the complexity and diversity of natural scenes, these traditional methods only perform well in certain types of scenes. To overcome this limitation, several researchers [2, 38, 40, 41] have attempted to propose universal methods that are directly applicable, valid for all scenes, have low hardware requirements, and are highly accurate. For example, Pierre-Luc et al. [40] used LBSP and RGB values to model pixel-level representations. Sajid [38] employed a background model bank comprising of multiple background models of the scene. Huaiye et al. [41] created a word consensus model called PAWCS by leveraging LBSP and color intensity, and Barnich et al. [2] proposed ViBe, which initializes the background model by assuming neighboring pixels share a similar temporal distribution. However, with the increasing number of videos on the Internet, the fitting capability of these manual algorithms is insufficient. Thus, it is reasonable to use learning-based methods to address these challenges, leading to the development of our LTS.

2.2. Deep Learning Methods

Deep neural networks have demonstrated excellent performance in scene understanding and analysis [1, 10, 14, 23, 29, 30, 32, 34, 35, 39, 45, 50, 51, 52, 53, 54]. It is reasonable to utilize deep learning networks to learn background scenes for moving object segmentation. For instance, Cascade CNN [49] uses image frames as input and outputs binary masks during network training. FgSegNet [30] incorporates a feature pyramid module to learn scene information, while MU-Net [36] leverages semantic segmentation to detect moving objects based on appearance cues. These

methods have achieved near-perfect results (with over 98% Fm values) on videos from standard datasets. However, their performance decrease significantly when applied to unseen videos due to their dependence on scene information. To improve the performance on unseen videos, the BSUV [45, 46] network employs content-modifying data augmentations during training, while 3DCD [32] estimates the background through a gradual reduction block. However, the uncertainty and computational cost associated with data augmentation still limit the use of such networks in real applications. In order to propose a universal network, GraphMOS [15] uses Graph neural network for moving object segmentation. AE-NE [39] employs a reconstruction loss function with background bootstrapping. Additionally, ADNN [54] learns the distribution of temporal information and achieves good results for both seen and unseen videos from various datasets, suggesting that distribution information may be a potential solution for universal moving object segmentation. Inspired by these excellent prior works, we propose learning temporal distributions and spatial correlations for moving object segmentation.

Our proposed LTS method has several important differences compared to ADNN [54], which result in over 15% improvement in accuracy. First, ADNN did not consider the possibility of learning spatial correlation to improve the binary mask, while LTS incorporates a Stochastic Bayesian Refinement network to learn spatial correlation. Second, LTS utilizes a defect iterative training strategy that allows the network to learn a better and globally optimized distribution information. Additionally, we also propose a better implementation in network architecture in which the infinitesimal issue in ADNN is alleviated. This new implementation achieves over 5% improvement in accuracy compared to ADNN. A more detailed discussion and comparisons are provided in Section 4 and supplementary material.

3. Methodology

3.1. Defect Iterative Distribution Learning

Compared to scene information, distribution information is less diverse. Thus, we assume that the distributions of temporal pixels in videos may be finite, making it possible to propose a single model to learn all distribution information from videos for moving object segmentation. However, even based on this assumption, the amount of distribution information is still enormous, making it prohibitively expensive to learn network parameters from all videos. To address this challenge, we propose the Defect Iterative Distribution Learning (DIDL) network. The training of the proposed DIDL network is unique. Instead of learning network parameters from the entire training set, we want to find a limited number of representative instances for training, thereby reducing the computational cost. The training

process of the proposed network is thus described as the process of using the network parameters $\hat{\theta}_i$ learned from a subset H_i sampled from the entire training set \mathbf{H} , to approximate the parameters θ learned from \mathbf{H} . Mathematically:

$$\theta = \operatorname{argmax}_{\hat{\theta}} \mathcal{L}(\hat{\theta}, \mathbf{H}) \simeq \mathbb{E}_{H_i \sim \mathbf{H}} (\operatorname{argmax}_{\hat{\theta}_i} \mathcal{L}(\hat{\theta}_i, H_i)), \quad (1)$$

where, \mathcal{L} is a maximum likelihood estimation used to describe the process of learning network parameters. In particular, the number of training instances in \mathbf{H} is much greater than the one for H_i , which means $\|H_i\|_0 \ll \|\mathbf{H}\|_0$. $\hat{\theta}_i$ is the network parameters learned from H_i which is sampled from \mathbf{H} .

During the training of the DIDL network, an initial subset H_1 is sampled¹ from the training set \mathbf{H} and used for initial training. After the network is trained into a local optimal by H_1 , a DIDL network with the estimated parameters $\hat{\theta}_1$ is used to validate the instances from the entire training set \mathbf{H} . During the validation, several instances are incorrectly classified and are used as the defective samples H_d . Next, the defective samples H_d from the validation process are merged into the subset H_1 to create a new subset, $H_2 = H_1 \cup H_d$, which is used for the next training iteration. With the proposed defect iterative training strategy, only the validation process involves the computation of \mathbf{H} , which saves a significant amount of computational resources. During experiments with the proposed approach, an NVIDIA RTX A4000 GPU with 16GB memory is sufficient for learning parameters from the training data with size of 3TB within 48 hours.

Due to page limitations, the details of the network architecture are provided in the supplementary material. The DIDL utilizes histograms of the differences between current pixels and their historical counterparts as the input. Mathematically:

$$\mathbf{H} = \{H_{x,y}(n)\} = \left\{ \frac{1}{T} \sum_{i=0}^T |I_i(x,y) - I_t(x,y)| \cap n \right\}_{x,y \in G} \quad (2)$$

where, $I_t(x,y)$ is the value of the pixel located at (x,y) and time t . T is the total number of frames. $H_{x,y}(n)$ is the histogram captured from pixel (x,y) , n is the index of the entries in the histograms. \mathbf{H} is the set of histograms which are used as the training set. The histograms obtained from the previous step are used as input for the product and sum distribution layers, where they are used to learn distribution information. A classification block consisting of ReLU and a fully connected layer is then attached to the output of the distribution layers. During the training process, the logistic loss on the final output node is minimized.

¹Sampled by Euclidean distance heuristic search. More details are given in the supplementary material.

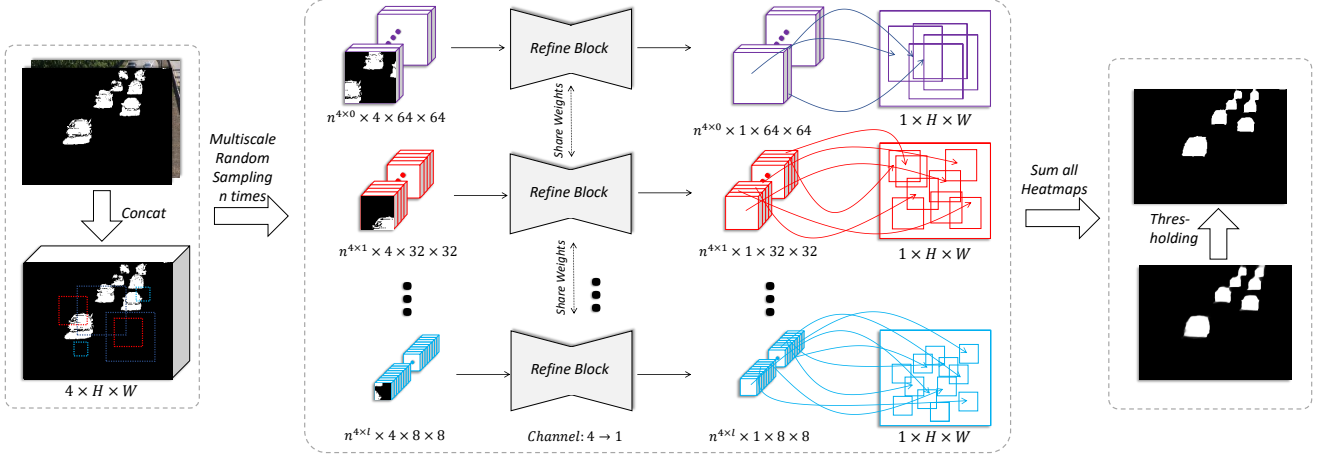


Figure 2: The framework of the Stochastic Bayesian Refinement network. To generate a refined foreground, the DIDL foreground output is merged with the corresponding image to a $4 \times H \times W$ tensor. The tensor is then sampled n times at varying scales to produce refined foreground patches, which are subsequently stacked to generate a heatmap. A threshold applied to this heatmap determines the refinement outcome.

For completeness, we briefly introduce the product distribution layer and sum distribution layer, please check [54] for more details. Both input, learning kernels and outputs for sum and product distribution layers are histogram, making it suitable for processing distributions represented by histograms. In particular, the product distribution layer is used to compute product of histograms in the input and learning kernels. Similarly, the sum distribution layer is used to compute the sum of histograms in the input and learning kernels. With the help of these two distribution layers, the proposed DIDL network can learn the distribution for moving object segmentation, with input of histograms of subtraction between the current frame and the historical frames. The output is the label of pixels, which can be mathematically shown as:

$$M(x, y) = \mathcal{C}(\mathcal{A}_{ri}(H_t(x, y))) \quad (3)$$

where, $H_t(x, y)$ is the histogram extracted from pixel (x, y) at time t . \mathcal{A}_{ri} is the arithmetic distribution layer. \mathcal{C} is the classification block.

3.2. Stochastic Bayesian Refinement Network

The DIDL network completely ignores spatial correlation, which could be beneficial for moving object segmentation, as neighboring pixels are expected to have similar labels. In order to improve segmentation accuracy, we propose the Stochastic Bayesian Refinement (SBR) network. The SBR network is a Bayesian inference process to relabel a pixel based on the information from its neighbourhood. Mathematically:

$$\begin{aligned} \hat{M}(x, y) &= \underset{a_i \in \{0,1\}}{\operatorname{argmax}} P(a_i | I(x, y)) \\ &= \underset{a_i}{\operatorname{argmax}} \frac{P(I(x, y) | a_i) P(a_i)}{P(I(x, y))} \\ &= \underset{a_i}{\operatorname{argmax}} \int_{g \in G} \frac{P(I(x, y) | g) P(g | a_i) P(a_i)}{P(I(x, y))} dg \end{aligned} \quad (4)$$

where, $\hat{M}(x, y)$ is the inferred label of a pixel located at (x, y) . $a_i \in \{0, 1\}$ denotes the label of a pixel belonging to the background or foreground. $I(x, y)$ is the value of a pixel located at (x, y) . $g \in G$ is the set of neighbouring pixels around (x, y) , and g is a single pixel inside G . Note that the size of G varies with respect to the resolution of images as well as object sizes. Unfortunately, the integral in Equation 4 includes the similarity $P(I(x, y) | g)$ between two pixels, which depends strongly on diverse spatial correlations among neighbouring pixels G . For instance, the Euclidean distance between two pixels is more appropriate for grayscale scenes. However, such advantages do not extend to thermal images, indicating that manually defined distance functions may not be universally applicable. Thus, it is reasonable to employ a network to approximate distance functions for inference. Mathematically:

$$\begin{aligned} f(I(x, y), a_i, G | \theta) &= \underset{a_i}{\operatorname{argmax}} \int_{g \in G} \frac{P(I(x, y) | g) P(g | a_i) P(a_i)}{P(I(x, y))} dg \\ &= \underset{a_i}{\operatorname{argmax}} P(a_i) \int_{g \in G} P(I(x, y) | g) P(g | a_i) dg \end{aligned} \quad (5)$$

where, $f(I(x, y), a_i, G | \theta)$ is our Stochastic Bayesian Network, and θ denotes the network parameters.

In order to capture the global optimized spatial correlation in a binary mask with the respect to an image, \hat{M} is compared with the groundtruth M for mathematical opti-

mization:

$$\begin{aligned}\hat{\theta} &= \operatorname{argmin}_{\theta} \int \int (\hat{M}(x, y) - M(x, y))^2 dx dy, \\ &= \operatorname{argmin}_{\theta} \int \int (f(I(x, y), a_i, G|\theta) - M(x, y))^2 dx dy,\end{aligned}\quad (6)$$

where, (x, y) is the location of a pixel in an image. As shown in Equation 6, there is overlap between the domain of the integral and G . Thus, we can simplify Equation 6 as follows:

$$\begin{aligned}\hat{\theta} &= \operatorname{argmin}_{\theta} \int \int (f(I(x, y), a_i, G|\theta) - M(x, y))^2 dx dy, \\ &= \operatorname{argmin}_{\theta} \frac{1}{N} \int \int_{x_1, y_1 \in G_1} (f(I(x_1, y_1), a_i, G_1|\theta) - M(x_1, y_1))^2 dx_1 dy_1 \\ &\quad + \frac{1}{N} \int \int_{x_2, y_2 \in G_2} (f(I(x_2, y_2), a_i, G_2|\theta) - M(x_2, y_2))^2 dx_2 dy_2 \cdots \\ &\quad + \frac{1}{N} \int \int_{x_N, y_N \in G_N} (f(I(x_N, y_N), a_i, G_N|\theta) - M(x_N, y_N))^2 dx_N dy_N \\ &= \operatorname{argmin}_{\theta} \frac{1}{N} \sum_{n=1}^N \int \int_{x, y \in G_n} (f(I(x, y), a_i, G_n|\theta) - M(x, y))^2 dx dy \\ &= \operatorname{argmin}_{\theta} \sum_{n=1}^N \int \int_{x, y \in G_n} (f(I(x, y), a_i, G_n|\theta) - M(x, y))^2 dx dy\end{aligned}\quad (7)$$

where, $\hat{\theta}$ denotes the estimated parameters of the SBR network. As shown in Equation 7, in order to get a globally optimized solution, (x, y) is sampled from G_n , and G_n is sample from the entire image. In particular, G_n is the group of neighbouring pixels around pixel (x_n, y_n) . (x_n, y_n) covers all the pixels in the image. Besides, the size of G_n also varies, which leads to an unacceptable computational cost. Thus, a stochastic solution such as the Monte-Carlo sampling [33] is suitable in this condition, which leads to the final optimal function of the proposed Stochastic Bayesian Refinement Network. Mathematically:

$$\begin{aligned}\hat{\theta} &\simeq \operatorname{argmin}_{\theta} \sum_{G_n \in \mathbf{G}} \sum_{x, y \in G_n} (f(I(x, y), a_i, G_n|\theta) - M(x, y))^2 \\ &\quad \text{where } f = \operatorname{argmax}_{a_i} P(a_i) \int_{g \in G} P(I(x, y)|g) P(g|a_i) dg\end{aligned}\quad (8)$$

where, (x, y) is the pixel that is sampled from G_n , which is sampled from the entire training image \mathbf{G} . The flowchart of our framework is demonstrated in Figure 2. In particular, the refinement block is an encoder-decoder architecture. To reduce the computational cost, a simplified U-net is utilized. With the motivation to find the global optimal from Equation 8, the patches must be randomly sampled at multiple scales because of the uncertainties of location (x, y) and the size of G . Without these considerations, the accuracy of our SBR network is reduced. To illustrate the aforementioned

point, we present ablation study in Section 4.3. Please refer to the supplementary material for the network architecture and implementation details.

4. Experimental Results

During the training of the proposed approach, 100 ground-truth frames from each video in CDNet2014 [48] are randomly selected. In addition, 5% of the total frames are sampled from videos in other datasets. Note that the number of training sets is less than or close to those for the most popular methods based on deep learning networks [15, 29, 36, 49]. In particular, one benefit of the proposed DIDL is reducing the computational cost, and not all instances are involved in training. For LTS-A, there are 1,157,286,920 (3,767 images if resolution is 480×640) histogram instances in total. However, only 62,630,630 (203 images) are involved for parameters optimization, constituting a mere 5% of the entire training set, which is less than 1% of all the datasets. Further details can be found in the supplementary material and public code.

To show the superiority of the proposed approach, we compare our method to several state-of-the-art methods, including ones that do not employ deep learning networks, such as PAWCS [41], SuBSENSE [40], CueV2 [3], Hai [19], IUTIS-5 [4], MBS [38], ShareM [8], WeSamBE [24], GMM [56], 3PDM [37], HMAO [27], B-SSSR [21], cDMD [12], SRPCA [22], DPGMM [17], TVRPCA [7], ViBe [2], RPCA [20], and methods based on deep learning networks ADNN [54], D-DPDL [53], BSUV-Net [46], BSUV2.0 [45], 3DCD-55 [32], AE-NE [39], DeepBS [1], CNN-SFC [10], DVTN [14], Cascade-CNN [49], FgSegNet [29], MU-NET [36], EDS-CNN [28], GraphMOS [15], DCP [43], MOD-GAN [44]. Comparing different models can be challenging due to variability in the experimental setup. To ensure a fair comparison, we train our models using three distinct settings: LTS-A (trained by all dataset), LTS-D (trained by target dataset), and LTS-U (trained by CDNet2014 [48] test on LASIESTA [9]). All three models have fixed parameters for testing, making them universal for moving object segmentation.

4.1. Unseen Video Results

A universal approach should be applicable to all videos, including those that are unseen. We train the LTS-U model on CDNet2014 [48] and evaluate it directly on LASIESTA [9], as shown in Table 1.

We can see that FgSegNet [29] performs remarkably well on known videos as shown in Table 2. However, its performance drops significantly to 0.37 for unseen videos, rendering it unsuitable for direct use in real applications. On the other hand, models such as BSUV [45] and AE-NE [39] are specifically designed for unseen videos. However, our method achieves promising results in unseen videos as

Table 1: Comparison of F-Measure Results for Videos in the LASIESTA Dataset [9].

Video	LTS-A	LTS-D	LTS-U	ADNN [54]	D-DP DL [53]	ADNN* [54]	BSUV 2.0 [45]	3DCD- 55 [32]	MSFS- 55 [30]	FgSeg Net [29]	AE- NE [39]	PAW CS [41]	SuBSE NSE [40]	CueV2 [3]	Hai [19]
Fix.	✓	✓	✓	×	×	✓	✓	×	×	×	✓	✓	✓	✓	✓
LSI	0.9836	0.9869	0.9229	0.9536	0.9142	0.9335	0.9200	0.8700	0.3900	0.5600	0.9100	0.9000	0.9000	0.8806	0.8876
LCA	0.9406	0.9310	0.7851	0.9504	0.9080	0.7316	0.6800	0.8200	0.4000	0.5500	0.8800	0.8800	0.8900	0.8444	0.8938
LOC	0.9844	0.9895	0.9447	0.9759	0.9694	0.9481	0.9600	0.9100	0.3700	0.6500	0.9100	0.9000	0.9500	0.7806	0.9223
LIL	0.9821	0.9888	0.5460	0.7661	0.8066	0.4869	0.8800	0.9200	0.3500	0.4200	0.8100	0.7900	0.6500	0.6488	0.8491
LMB	0.9863	0.9921	0.9400	0.9802	0.9447	0.9262	0.8100	0.8900	0.6400	0.5600	0.9200	0.8100	0.7700	0.9374	0.8440
LBS	0.9796	0.9861	0.8898	0.9707	0.7275	0.8884	0.7700	0.7200	0.3600	0.1900	0.7900	0.7900	0.7300	0.6644	0.6809
O.CL	0.9870	0.9901	0.9435	0.9814	0.9796	0.9534	0.9300	0.8700	0.4100	0.2800	0.9400	0.9600	0.9200	0.9276	0.8267
O.RA	0.9734	0.9870	0.9356	0.9868	0.9437	0.8744	0.9400	0.9000	0.3500	0.1800	0.8000	0.9300	0.9000	0.8669	0.8908
O.SN	0.9772	0.9891	0.8451	0.9647	0.9516	0.8327	0.8400	0.6900	0.3100	0.0100	0.8200	0.6900	0.8100	0.7786	0.1740
O.SU	0.9558	0.9773	0.8949	0.9300	0.9226	0.8829	0.7900	0.8500	0.3700	0.3300	0.9100	0.8200	0.7900	0.7221	0.8568
Average	0.9750	0.9806	0.8648	0.9460	0.9068	0.8459	0.8500	0.8400	0.4000	0.3700	0.8690	0.8470	0.8327	0.8051	0.7826

ADNN: Networks are trained and tested on individual videos.

ADNN*: Network is trained on CDNet and test on LASIESTA.

Fix. : Fixed parameters

well, being only 0.004 below AE-NE. The differences are AE-NE needs training on unseen scenes before being used and BSUV involves a data argumentation process for unseen videos, which allows the authors to tune parameters to fit the tested scenes. Our aim is to propose a directly usable universal model, where seen or unseen videos are of secondary importance, since what users need is a model that can be used out of a box. In this regard, we also present results for LTS-A and LTS-D, which achieve promising results.

4.2. Universal Moving Object Segmentation Results

Despite the lack of a gold standard definition for universal moving object segmentation methods, prior studies [2, 38, 40, 41, 54] suggest that a universal model should not only exhibit high performance on diverse test videos, but it should also be directly applicable. Most traditional methods [38, 40, 41, 56] are considered universal because they can be used directly with fixed or adaptive parameters. In contrast, our method also has fixed parameters and significantly outperforms them in terms of accuracy. Our comparisons can be considered reasonable, since the results of traditional methods also involve human knowledge. For example, the parameters of GMM, such as the number of Gaussian functions, are adjusted by Zivkovic et al. [56] with reference to ground-truth frames. By contrast, in methods based on deep learning networks, ground-truth is directly input into networks for learning. In addition, some networks are difficult to consider as universal methods, given their dependence on scene information. For example, although FgSegNet [29, 13] achieves near-perfect performance on CDNet2014 [48], it utilizes a distinct network for each video and changes the parameters based on the groundtruth frames. This results in a significant drop in performance on LASIESTA [9]. Similar issues also exist in MU-Net [36], Cascade-CNN [49], DVTN [14]. Although unsupervised or semi-supervised learning solutions

[15, 39] are suitable for various scenarios, they face challenges in becoming universal methods due to network setup, prolonged training processes, and performance reduction for diverse videos. Compared to these methods, the proposed approach achieves better results and is directly applicable. One could feel frustrated when using moving ob-



Figure 3: LTS is a universal approach that can be applied to a wide range of real-life scenarios. Red masks represent the moving objects. None of these scenes are in the training. Object segmentation applications on their phone, discouraged by the considerable amount of time for network training. Thus, it is crucial to have a universal network that can be applied without additional parameter tuning, as suggested in ADNN [54]. We employ the same strategy, where the parameters are kept constant for all tested videos, as presented in Tables 1, 2, 3 and 4, to provide a universal solution. Our approach achieves favorable results with fixed parameters across all four datasets. Specifically, on CDNet2014 [48], our approach performs well compared to the other methods with fixed parameters. Despite our inspiration being drawn from ADNN [54], we improve results by 15%. This demonstrates the contributions of the proposed approach including Defect Iterative Distribution Learning and Stochastic Bayesian Refinement Network². Furthermore, the results for LTS-A and LTS-D in Table 1 and Table 2, respectively, demonstrate the universality of our approach, as they exhibit almost the same performance.

Given the limited scope and subject matter in standard

Table 2: Comparison of F-Measure Results Over the Videos of CDNet2014 Dataset [48].

Method	Fix.	Baseline	Dyn. Bg.	Cam. Jitt.	Int. Mit.	Shadow	Ther.	Bad Wea.	Low Fr.	Nig. Vid.	PTZ	Turbul.	Average
IUTIS-5 [4]	✓	0.9567	0.8902	0.8332	0.7296	0.9084	0.8303	0.8248	0.7743	0.5290	0.4282	0.7836	0.7717
MBS [38]	✓	0.9287	0.7915	0.8367	0.7568	0.7968	0.8194	0.7980	0.6350	0.5158	0.5520	0.5858	0.7288
PAWCS [41]	✓	0.9397	0.8938	0.8137	0.7764	0.8913	0.8324	0.8152	0.6588	0.4152	0.4615	0.6450	0.7403
ShareM [8]	✓	0.9522	0.8222	0.8141	0.6727	0.8898	0.8319	0.8480	0.7286	0.5419	0.3860	0.7339	0.7474
SuBSENSE [40]	✓	0.9503	0.8177	0.8152	0.6569	0.8986	0.8171	0.8619	0.6445	0.5599	0.3476	0.7792	0.7408
WeSamBE [24]	✓	0.9413	0.7440	0.7976	0.7392	0.8999	0.7962	0.8608	0.6602	0.5929	0.3844	0.7737	0.7446
GMM [56]	✓	0.8245	0.6330	0.5969	0.5207	0.7370	0.6621	0.7380	0.5373	0.4097	0.1522	0.4663	0.5707
3PDM [37]	✓	0.8820	0.8990	0.7270	0.6860	0.8650	0.8410	0.8280	0.5350	0.4210	0.5010	0.7930	0.7253
HMAO [27]	✓	0.8200	N/A	0.6300	0.7200	0.8600	0.8400	0.7900	0.6000	0.3600	N/A	0.4600	N/A
B-SSSR [21]	✓	0.9700	0.9500	0.9300	0.7400	0.9300	0.8600	0.9200	N/A	N/A	N/A	0.8700	N/A
DeepBS [1]	×	0.9580	0.8761	0.8990	0.6098	0.9304	0.7583	0.8301	0.6002	0.5835	0.3133	0.8455	0.7548
CNN-SFC [10]	×	0.9497	0.9035	0.8035	0.7499	0.9127	0.8494	0.9084	0.7808	0.6527	0.7280	0.8288	0.8243
DPDL-40 [53]	×	0.9692	0.8692	0.8661	0.8759	0.9361	0.8379	0.8688	0.7078	0.6110	0.6087	0.7636	0.8106
BSUV-Net [46]	×	0.9640	0.8176	0.7788	0.7601	0.9664	0.8455	0.8730	0.6788	0.6815	0.6562	0.7631	0.7986
BSUV-Net2 [45]	×	0.9620	0.9057	0.9004	0.8263	0.9562	0.8932	0.8844	0.7902	0.5857	0.7037	0.8174	0.8387
DVTN [14]	×	0.9811	0.9329	0.9014	0.9595	0.9467	0.9479	0.8780	0.7818	0.7737	0.5957	0.9034	0.8789
ADNN [54]	×	0.9797	0.9454	0.9411	0.9114	0.9537	0.9411	0.9038	0.8123	0.6940	0.7424	0.8806	0.8826
Cas.CNN [49]	×	0.9700	0.9500	0.9700	0.8700	0.9500	0.8900	0.7900	0.7400	0.8700	0.8800	0.8400	0.8836
EDS-CNN [28]	×	0.9586	0.9112	0.8990	0.8780	0.8565	0.8048	0.8757	0.9321	0.7715	N/A	0.7573	0.8644
FgSegNet [29]	×	0.9975	0.9939	0.9945	0.9933	0.9954	0.9923	0.9838	0.9558	0.9779	0.9893	0.9776	0.9864
ADNN* [54]	✓	0.9562	0.8748	0.8532	0.8742	0.9347	0.8568	0.8764	0.7983	0.6161	0.2409	0.7826	0.7876
AE-NE [39]	✓	0.8959	0.6225	0.9230	0.8231	0.8947	0.7999	0.8337	0.6771	0.5172	0.8000	0.8382	0.7841
MU-NET [36]	✓	0.9875	0.9836	0.9802	0.9872	0.9825	0.9825	0.9319	0.7237	0.8575	0.7946	0.8499	0.9146
GraphMOS [15]	✓	0.9710	0.8922	0.9233	0.6455	0.9901	0.9010	0.9411	0.6910	0.8211	0.8511	0.8233	0.8592
LTS-A (our)	✓	0.9906	0.9710	0.9767	0.9787	0.9889	0.9790	0.9759	0.8382	0.8637	0.8302	0.9567	0.9431
LTS-D (our)	✓	0.9898	0.9690	0.9758	0.9821	0.9881	0.9818	0.9767	0.8576	0.8725	0.8630	0.9590	0.9484

Dyn. Bg. : Dynamic Background, Cam. Jitt. : Camera Jitter, Int. Mit. : Intermittent Object Motion, Ther. : Thermal, Bad Wea. : Bad Weather, Low Fr. : Low Framerate, Nig. Vid. : Night Videos, and Turbul. : Turbulence. Fix. : Fixed Parameters, ADNN* : ADNN fixed parameters version.

Table 3: Comparison of F-Measure results for videos in the BMC dataset [47].

Method	Fix.	1	2	3	4	5	6	7	8	9	Ave.
SuBSENSE[40]	✓	0.70	0.62	0.83	0.69	0.21	0.76	0.53	0.68	0.83	0.65
cDMD[12]	✓	0.56	0.68	0.77	0.73	0.57	0.64	0.76	0.51	0.57	0.64
SRPCA[22]	✓	0.79	0.74	0.83	0.81	0.80	0.69	0.70	0.84	0.86	0.78
DPGMM[17]	✓	0.72	0.69	0.75	0.80	0.71	0.68	0.65	0.78	0.79	0.73
TVRPCA[7]	✓	0.76	0.67	0.68	0.82	0.77	0.69	0.71	0.79	0.88	0.75
PAWCS[41]	✓	0.70	0.58	0.85	0.72	0.27	0.79	0.58	0.74	0.80	0.67
DCP[43]	✓	0.58	0.62	0.59	0.71	0.67	0.69	0.65	0.70	0.70	0.66
AE-NE[39]	✓	0.81	0.72	0.78	0.78	0.60	0.73	0.32	0.84	0.77	0.71
MOD-GAN[44]	✓	0.80	0.75	0.69	0.70	0.87	0.66	0.71	0.75	0.80	0.75
LTS-A (our)	✓	0.82	0.90	0.83	0.86	0.76	0.84	0.87	0.80	0.79	0.83

Fix. : Fixed Parameters. Ave. : Average.

datasets, videos included may not provide a fully representative sample of real-world videos. Furthermore, the number of segmented objects in these datasets is limited, making it challenging to rely solely on scene information to handle dynamic and complex scenarios encountered in the real world. As shown in Figure 3, to further substantiate the universality of our approach, we gathered a corpus of 128 videos containing 298k frames that were recorded in real-life scenarios or obtained from cameras located worldwide, featuring diverse scenes ². In practical scenarios, LTS exhibits two distinctive benefits. First, LTS can handle the segmentation of objects that are not presented in the train-

²Please refer to the supplementary material for details.

ing phase, such as animals. Second, LTS performs segmentation solely on objects that are in motion, avoiding the erroneous segmentation of stationary objects (e.g., a car waiting at a traffic light). The video results on real-world scenarios can be found online³.

4.3. Ablation Study and Discussion

Ablation Study: This section presents the results of an ablation study conducted on four datasets, presented in Table 5. On the CDNet2014 [48] dataset, DIDL-A achieves an Fm score of 0.7368. When refined by SBR without random sampling and multi-scale, the improvement in accuracy is negligible, resulting in a Fm score of 0.7372 as shown in LTS-A *w/o* R&M. In contrast, the multiscale strategy significantly improves accuracy, as demonstrated by the Fm score of 0.9023 in LTS-A *w/o* R, while the multi-scale and random sampling strategy further improves accuracy, as shown by the Fm score of 0.9431 in LTS-A. Interestingly, when the size of G in Equation 8 is maximized to the image size, the input of the SBR network becomes a combination of the image frame and foreground mask, which is similar to MU-Net2 [36]. This observation indicates that MU-Net2 can be considered as a specific condition of the proposed SBR network. Unfortunately, this specific condition removes both

³Sample videos are available in the supplementary material. The complete 2-hour video will be released after the acceptance of the paper.

Table 4: Comparison of F-Measure results for videos in the SBMI2015 dataset [31].

Method	Fix.	Board	Cand.	CAVI.1	CAVI.2	CaVig.	Foliage	HallA.	High.I	High.II	Hum.B.	IBM.2	Peop.A.	Snel.	Ave.
ViBe [2]	✓	0.7377	0.5020	0.8051	0.7347	0.3497	0.5539	0.6017	0.4150	0.5554	0.4268	0.7001	0.6111	0.3083	0.5617
RPCA [20]	✓	0.5304	0.4730	0.4204	0.1933	0.4720	0.4617	0.4525	0.5733	0.7335	0.5765	0.6714	0.3924	0.4345	0.4911
SubSENSE [40]	✓	0.6588	0.6959	0.8783	0.8740	0.4080	0.1962	0.7559	0.5073	0.8779	0.8560	0.9281	0.4251	0.2467	0.6391
FgSN-M-55 [29]	✓	0.8900	0.2100	0.7000	0.0500	0.5700	0.9100	0.7100	0.7500	0.3100	0.8300	0.8300	0.9000	0.5200	0.6292
MSFS-55 [25]	✓	0.9100	0.2600	0.5700	0.0800	0.5700	0.8000	0.5200	0.8200	0.5800	0.6100	0.6000	0.8700	0.6800	0.6054
3DCD-55 [32]	✓	0.8300	0.3500	0.7900	0.5600	0.4800	0.6900	0.5800	0.7300	0.7700	0.6500	0.7000	0.7800	0.7600	0.6669
BSUV2.0 [45]	✓	0.9886	0.8597	0.9358	0.8649	0.4773	0.3450	0.9346	0.8337	0.9592	0.9503	0.9643	0.6930	0.3786	0.7834
GraphMOS [15]	✓	0.9931	0.7551	0.9744	0.9210	0.7322	0.7792	0.9122	0.9880	0.9547	0.9522	0.9856	0.9059	0.7380	0.8917
ADNN* [54]	✓	0.4527	0.5222	0.9169	0.8429	0.7259	0.0722	0.8200	0.7493	0.9827	0.9431	0.9348	0.3071	0.0445	0.6395
ADNN [54]	×	0.9421	0.9242	0.9550	0.8865	0.9589	0.7528	0.9151	0.8689	0.9854	0.9525	0.9548	0.7108	0.7893	0.8920
LTS-A (our)	✓	0.9932	0.9848	0.9940	0.9432	0.9775	0.9670	0.9773	0.9741	0.9915	0.9616	0.9795	0.9891	0.9775	0.9751

Cand. : Candela.m1.10, CAVI.1 : CAVIAR1, CAVI.2 : CAVIAR2, CaVig. : CaVignal, HallA. : HallAndMonitor, High.I : HighwayI, High.II : HighwayII, Hum.B. : HumanBody2, IBM.2 : IBMtest2, Prop.A. : PeopleAndFoliage, Snel. : Snellen, Fix. : Fixed Parameters, Ave. : Average, ADNN*: ADNN fixed parameters version.

Table 5: Ablation Study and Comparison of LTS on Different Datasets using Fm Score.

Method	Fix.	Net. Size	CDNet 2014[48]	LASI ESTA[9]	SBMI 2015[31]	BMC [47]
DIDL-D	×	0.45MB	0.7691	0.9174	N/A	N/A
LTS-D	×	1.37MB	0.9485	0.9807	N/A	N/A
DIDL-A	✓	0.45MB	0.7368	0.8936	0.8872	0.6890
LTS-A w/o R&M	✓	1.37MB	0.7372	0.8726	0.8923	0.6705
LTS-A w/o R	✓	1.37MB	0.9023	0.9538	0.9625	0.7823
LTS-A	✓	1.37MB	0.9431	0.9750	0.9751	0.8317
LTS-U	✓	1.37MB	N/A	0.8648	N/A	N/A
DIDL-U	✓	0.45MB	N/A	0.7961	N/A	N/A
DIDL-U+MU2 [36]	✓	68.41MB	N/A	0.7303	N/A	N/A
DIDL-A+MU2 [36]	✓	68.41MB	0.8955	0.7706	0.8325	0.6456
GMM [55]	✓	N/A	0.5566	N/A	N/A	N/A
GMM+SBR	✓	0.92MB	0.6799	N/A	N/A	N/A
Noise+SBR	✓	0.92MB	0.0482	0.0352	0.0519	0.0123
ADNN [54]	✓	0.42MB	0.7877	0.8459	0.6396	N/A
AE-NE [39]	×	N/A	0.7841	0.8690	N/A	0.7100
GraphMOS [15]	×	N/A	0.8592	N/A	0.7834	N/A
BSUV2.0 [45]	×	115.94MB	0.8387	0.8500	0.8917	N/A
FgSegNet [29]	×	56.16MB	0.9864	0.3700	N/A	N/A
MU-Net1 [36]	✓	67.96MB	0.9146	0.2656	0.4347	0.3002
EDS-Net [28]	×	18.64MB	0.8644	N/A	N/A	N/A

DIDL-{A/D/U}: The LTS-{A/D/U} results without Bayesian refinement network.

w/o R&M: without multiscale random sampling in Bayesian refinement network.

w/o R: without random sampling in Bayesian refinement network.

Fix. : Fixed parameters, Net. Size: The size of network.

For network size, all implementations are in Pytorch.

multi-scale and random sampling, leading to overfitting to scene information and poor performance on diverse videos. To demonstrate this, we directly input DIDL results into a pre-trained MU-Net2 provided by the author, presenting the results of DIDL-A+MU2 and DIDL-U+MU2, which even worsens results of the original DIDL-A/DIDL-U. Moreover, SBR can be directly applied to other methods such as GMM [55] and the results of GMM+SBR show that incorporating spatial information improves segmentation accuracy. Additionally, despite being trained on 97 videos simultaneously, LTS-A's accuracy is only slightly lower than LTS-D, indicating the universality of our approach. Finally, to confirm that our SBR network is refined by spatial information rather than scene information, we directly concatenate noise foreground with the image into SBR, resulting in poor performance (Noise+SBR).

We also compare with state-of-the-art methods, consid-

ering both network size and accuracy. We determine the net size by reporting pre-trained model file sizes. Our method has the second-smallest network in terms of file size, next to ADNN [54]. However, the proposed approach achieves significantly higher accuracy than ADNN. During testing on Nvidia RTX3090, our method takes only 0.15 seconds per frame (240×360 resolution) excluding I/O time. Notably, our approach requires only 2GB of memory, making it compatible with low-end computers.

Discussion: According to a comprehensive review of moving object segmentation in stationary cameras (Section 9 and 10, Page 59) [6], different architectures should be used in different scenarios and tasks. For example, supervised networks like FgSegNet [29] is useful when labeled groundtruth is available, while unsupervised methods like GraphMOS [15] can be used if groundtruth is limited. However, from our point of view, the potential of deep learning networks may be beyond this. With proper network design, it may be possible to propose a single network that can handle all scenarios in real-life environments. Thus, LTS-A is proposed. In addition to the excellent performance of LTS-A on four standard datasets containing 97 videos, we also applied LTS-A to another 128 videos in real-life scenarios, which are available in the supplementary material. Although quantitative results are not available due to a lack of groundtruth, the qualitative results are promising. Both of these demonstrate the potential of our approach to be a universal method for moving object segmentation.

There are some limitations in the proposed approaches. In addition to the processing time for high-resolution images, Equation 7 suggests that both the sampling position and size should be random. However, this leads to high computation cost. As a compromise, we use fixed sizes of 16×16 , 32×32 , and 64×64 in our implementation. This limitation warrants further investigation in future research.

5. Conclusion

We proposed a potential solution for universal moving object segmentation by learning the temporal pixel distribution and the spatial correlation (LTS). To learn the pixel distribution, we improved the implementation of the prod-

uct distribution layer and introduced Defect Iterative Distribution Learning (DIDL) to learn parameters from entire training set by using a subset of instances. In order to take advantage of spatial correlation, we proposed the Stochastic Bayesian Refinement (SBR) Network to further improve results. Compared to previous methods, our approach enables direct testing on any video using fixed model parameters. Additionally, our approach has less parameters, low computational requirements, high accuracy, and is user-friendly. Thus, our method is a promising approach for universal moving object segmentation.

References

- [1] Mohammadreza Babaei, Duc Tung Dinh, and Gerhard Rigoll. A deep convolutional neural network for video sequence background subtraction. *Pattern Recognit.*, pages 635 – 649, 2018. 2, 5, 7
- [2] Olivier Barnich and Marc Van Droogenbroeck. Vibc: A universal background subtraction algorithm for video sequences. *IEEE Transactions on Image processing*, 20(6):1709–1724, 2010. 2, 5, 6, 8
- [3] Daniel Berjón, Carlos Cuevas, Francisco Morán, and Narciso García. Real-time nonparametric background subtraction with tracking-based foreground update. *Pattern Recognition*, 74:156–170, 2018. 2, 5, 6
- [4] Simone Bianco, Gianluigi Ciocca, and Raimondo Schettini. How far can you get by combining change detection algorithms? In *Int. Conf. Image Analysis and Process.*, 2017. 2, 5, 7
- [5] Thierry Bouwmans, Fida El Baf, and Bertrand Vachon. Statistical background modeling for foreground detection: A survey. In *Handbook of pattern recognition and computer vision*, pages 181–199. World Scientific, 2010. 2
- [6] Thierry Bouwmans, Sajid Javed, Maryam Sultana, and Soon Ki Jung. Deep neural network concepts for background subtraction: A systematic review and comparative evaluation. *Neural Networks*, 117:8–66, 2019. 8
- [7] Xiaochun Cao, Liang Yang, and Xiaojie Guo. Total variation regularized rpca for irregularly moving object detection under dynamic background. *IEEE transactions on cybernetics*, 46(4):1014–1027, 2015. 2, 5, 7
- [8] Yingying Chen, Jinqiao Wang, and Hanqing Lu. Learning sharable models for robust background subtraction. In *IEEE Int. Conf. Multimedia and Expo (ICME)*, pages 1–6, June 2015. 2, 5, 7
- [9] Carlos Cuevas, Eva María Yáñez, and Narciso García. Labeled dataset for integral evaluation of moving object detection algorithms: Lasiesta. *Computer Vision and Image Understanding*, 152:103–117, 2016. 5, 6, 8
- [10] Arjan Kuijper Dongdong Zeng, Ming Zhu. Combining background subtraction algorithms with convolutional neural network. *Journal of Electronic Imaging*, (1):1 – 6 – 6, 2019. 2, 5, 7
- [11] S. E. Ebadi and E. Izquierdo. Foreground segmentation with tree-structured sparse rpca. *IEEE Trans. Pattern Anal. Mach. Intell.*, Sep. 2018. 2
- [12] N Benjamin Erichson, Steven L Brunton, and J Nathan Kutz. Compressed dynamic mode decomposition for background modeling. *Journal of Real-Time Image Processing*, 16:1479–1492, 2019. 2, 5, 7
- [13] Fei Gao, Yunyang Li, and Shufang Lu. Extracting moving objects more accurately: a cda contour optimizer. *IEEE Transactions on Circuits and Systems for Video Technology*, 31(12):4840–4849, 2021. 6
- [14] Y. Ge, J. Zhang, X. Ren, C. Zhao, J. Yang, and A. Basu. Deep variation transformation network for foreground detection. *IEEE Transactions on Circuits and Systems for Video Technology*, pages 1–1, 2020. 2, 5, 6, 7
- [15] J. H. Giraldo, S. Javed, and T. Bouwmans. Graph moving object segmentation. *IEEE Transactions on Pattern Analysis and Machine Intelligence*, pages 1–1, 2022. 3, 5, 6, 7, 8
- [16] Kalpana Goyal and Jyoti Singhai. Review of background subtraction methods using gaussian mixture model for video surveillance systems. *Artificial Intelligence Review*, 50:241–259, 2018. 2
- [17] Tom SF Haines and Tao Xiang. Background subtraction with dirichletprocess mixture models. *IEEE transactions on pattern analysis and machine intelligence*, 36(4):670–683, 2013. 5, 7
- [18] Tom S.F. Haines and Tao Xiang. Background subtraction with dirichletprocess mixture models. *IEEE Transactions on Pattern Analysis and Machine Intelligence*, 36(4):670–683, 2014. 2
- [19] T. S. F. Haines and T. Xiang. Background subtraction with dirichletprocess mixture models. *IEEE Trans. Pattern Anal. Mach. Intell.*, (4):670–683, April 2014. 2, 5, 6
- [20] Michael Harville, Gaile Gordon, and John Woodfill. Foreground segmentation using adaptive mixture models in color and depth. In *Proceedings IEEE workshop on detection and recognition of events in video*, pages 3–11. IEEE, 2001. 5, 8
- [21] S. Javed, A. Mahmood, S. Al-Maadeed, T. Bouwmans, and S. K. Jung. Moving object detection in complex scene using spatiotemporal structured-sparse rpca. *IEEE Trans. Image Process.*, Feb 2019. 2, 5, 7
- [22] Sajid Javed, Arif Mahmood, Thierry Bouwmans, and Soon Ki Jung. Spatiotemporal low-rank modeling for complex scene background initialization. *IEEE Transactions on Circuits and Systems for Video Technology*, 28(6):1315–1329, 2016. 2, 5, 7
- [23] Ge-Peng Ji, Keren Fu, Zhe Wu, Deng-Ping Fan, Jianbing Shen, and Ling Shao. Full-duplex strategy for video object segmentation. In *Proceedings of the IEEE/CVF international conference on computer vision*, pages 4922–4933, 2021. 2
- [24] S. Jiang and X. Lu. Wesambe: A weight-sample-based method for background subtraction. *IEEE Trans. Circuits Syst. Video Technol.*, (99):1–1, 2017. 2, 5, 7
- [25] Zhao Kang, Chong Peng, and Qiang Cheng. Robust pca via nonconvex rank approximation. In *2015 IEEE International Conference on Data Mining*, pages 211–220. IEEE, 2015. 8
- [26] Dar-Shyang Lee. Effective gaussian mixture learning for video background subtraction. *IEEE Transactions on Pattern Analysis and Machine Intelligence*, 27(5):827–832, 2005. 2

- [27] L. Li, Q. Hu, and X. Li. Moving object detection in video via hierarchical modeling and alternating optimization. *IEEE Transactions on Image Processing*, pages 2021–2036, 2019. 2, 5, 7
- [28] Kyungsun Lim, Won-Dong Jang, and Chang-Su Kim. Background subtraction using encoder-decoder structured convolutional neural network. In *2017 14th IEEE international conference on advanced video and signal based surveillance (AVSS)*, pages 1–6. IEEE, 2017. 5, 7, 8
- [29] Long Ang Lim and Hacer Yalim Keles. Foreground segmentation using convolutional neural networks for multiscale feature encoding. *Pattern Recognition Letters*, 112:256–262, 2018. 1, 2, 5, 6, 7, 8
- [30] Long Ang Lim and Hacer Yalim Keles. Learning multi-scale features for foreground segmentation. *Pattern Analysis and Applications*, 23(3):1369–1380, 2020. 2, 6
- [31] Lucia Maddalena and Alfredo Petrosino. Towards benchmarking scene background initialization. In *New Trends in Image Analysis and Processing-ICIAP 2015 Workshops*, pages 469–476. Springer, 2015. 8
- [32] Murari Mandal, Vansh Dhar, Abhishek Mishra, Santosh Kumar Vipparthi, and Mohamed Abdel-Mottaleb. 3dcd: Scene independent end-to-end spatiotemporal feature learning framework for change detection in unseen videos. *IEEE transactions on image processing*, 30:546–558, 2020. 2, 3, 5, 6, 8
- [33] Shakir Mohamed, Mihaela Rosca, Michael Figurnov, and Andriy Mnih. Monte carlo gradient estimation in machine learning. *The Journal of Machine Learning Research*, 21(1):5183–5244, 2020. 5
- [34] Víctor Manuel Mondéjar-Guerra, José Rouco, Jorge Novo, and Marcos Ortega. An end-to-end deep learning approach for simultaneous background modeling and subtraction. In *BMVC*, 2019. 2
- [35] Duo Peng, Yinjie Lei, Wen Li, Pingping Zhang, and Yulan Guo. Sparse-to-dense feature matching: Intra and inter domain cross-modal learning in domain adaptation for 3d semantic segmentation. In *Proceedings of the IEEE/CVF International Conference on Computer Vision*, pages 7108–7117, 2021. 2
- [36] Gani Rahmon, Filiz Bunyak, Guna Seetharaman, and Kannappan Palaniappan. Motion u-net: multi-cue encoder-decoder network for motion segmentation. In *2020 25th International Conference on Pattern Recognition (ICPR)*, pages 8125–8132. IEEE, 2021. 2, 5, 6, 7, 8
- [37] S. M. Roy and A. Ghosh. Foreground segmentation using adaptive 3 phase background model. *IEEE Transactions on Intelligent Transportation Systems*, pages 2287–2296, 2020. 2, 5, 7
- [38] H. Sajid and S. C. S. Cheung. Universal multimode background subtraction. *IEEE Trans. Image Process.*, (7):3249–3260, July 2017. 2, 5, 6, 7
- [39] Bruno Sauvalle and Arnaud de La Fortelle. Autoencoder-based background reconstruction and foreground segmentation with background noise estimation. In *Proceedings of the IEEE/CVF Winter Conference on Applications of Computer Vision*, pages 3244–3255, 2023. 2, 3, 5, 6, 7, 8
- [40] P. L. St-Charles, G. A. Bilodeau, and R. Bergevin. Subsense: A universal change detection method with local adaptive sensitivity. *IEEE Trans. Image Process.*, (1):359–373, Jan 2015. 2, 5, 6, 7, 8
- [41] P. L. St-Charles, G. A. Bilodeau, and R. Bergevin. Universal background subtraction using word consensus models. *IEEE Trans. Image Process.*, (10):4768–4781, Oct 2016. 2, 5, 6, 7
- [42] Chris Stauffer and W Eric L Grimson. Adaptive background mixture models for real-time tracking. In *Proceedings. 1999 IEEE computer society conference on computer vision and pattern recognition (Cat. No PR00149)*, volume 2, pages 246–252. IEEE, 1999. 2
- [43] Maryam Sultana, Arif Mahmood, Sajid Javed, and Soon Ki Jung. Unsupervised deep context prediction for background estimation and foreground segmentation. *Machine Vision and Applications*, 30:375–395, 2019. 5, 7
- [44] Maryam Sultana, Arif Mahmood, and Soon Ki Jung. Unsupervised moving object detection in complex scenes using adversarial regularizations. *IEEE Transactions on Multimedia*, 23:2005–2018, 2020. 5, 7
- [45] M Ozan Tezcan, Prakash Ishwar, and Janusz Konrad. Bsv-net 2.0: Spatio-temporal data augmentations for video-agnostic supervised background subtraction. *IEEE Access*, 9:53849–53860, 2021. 2, 3, 5, 6, 7, 8
- [46] Ozan Tezcan, Prakash Ishwar, and Janusz Konrad. Bsv-net: A fully-convolutional neural network for background subtraction of unseen videos. In *WACV*, March 2020. 3, 5, 7
- [47] Antoine Vacavant, Thierry Chateau, Alexis Wilhelm, and Laurent Lequievre. A benchmark dataset for outdoor foreground/background extraction. In *Computer Vision-ACCV 2012 Workshops*, pages 291–300. Springer, 2013. 7, 8
- [48] Yi Wang, Pierre-Marc Jodoin, Fatih Porikli, Janusz Konrad, Yannick Benezeth, and Prakash Ishwar. Cdnets 2014: An expanded change detection benchmark dataset. In *Proceedings of the IEEE conference on computer vision and pattern recognition workshops*, pages 387–394, 2014. 5, 6, 7, 8
- [49] Yi Wang, Zhiming Luo, and Pierre-Marc Jodoin. Interactive deep learning method for segmenting moving objects. *Pattern Recognition Letters*, 96:66–75, 2017. 2, 5, 6, 7
- [50] Siming Yan, Zhenpei Yang, Chongyang Ma, Haibin Huang, Etienne Vouga, and Qixing Huang. Hpnet: Deep primitive segmentation using hybrid representations. In *Proceedings of the IEEE/CVF International Conference on Computer Vision*, pages 2753–2762, 2021. 2
- [51] Charig Yang, Hala Lamdouar, Erika Lu, Andrew Zisserman, and Weidi Xie. Self-supervised video object segmentation by motion grouping. In *Proceedings of the IEEE/CVF International Conference on Computer Vision*, pages 7177–7188, 2021. 2
- [52] Yuhang Zang, Chen Huang, and Chen Change Loy. Fasa: Feature augmentation and sampling adaptation for long-tailed instance segmentation. In *Proceedings of the IEEE/CVF International Conference on Computer Vision*, pages 3457–3466, 2021. 2
- [53] C. Zhao, T. Cham, X. Ren, J. Cai, and H. Zhu. Background subtraction based on deep pixel distribution learning. In *IEEE Int. Conf. Multimedia and Expo (ICME)*, July 2018. 2, 5, 6, 7

- [54] Chenqiu Zhao, Kangkang Hu, and Anup Basu. Universal background subtraction based on arithmetic distribution neural network. *IEEE Transactions on Image Processing*, 31:2934–2949, 2022. [2](#), [3](#), [4](#), [5](#), [6](#), [7](#), [8](#)
- [55] Z. Zivkovic. Improved adaptive gaussian mixture model for background subtraction. In *Proceedings of the 17th International Conference on Pattern Recognition, 2004. ICPR 2004.*, volume 2, pages 28–31 Vol.2, 2004. [2](#), [8](#)
- [56] Z. Zivkovic. Improved adaptive gaussian mixture model for background subtraction. In *Int. Conf. Pattern Recognit. (ICPR)*, 2004. [5](#), [6](#), [7](#)